

Article

Exploring the Excited-State Nonadiabatic Effects in the Semisaturated Planar Tetracoordinated Carbon Molecule C_7H_4

Chithra Mohan Jayakumari , Probal Nag, Sai Vamsi Krishna Isukapalli  and Sivaranjana Reddy Vennapusa * 

School of Chemistry, Indian Institute of Science Education and Research Thiruvananthapuram, Maruthamala P.O., Vithura, Thiruvananthapuram 695551, India; chithramj17@iisertvm.ac.in (C.M.J.); probalnag17@iisertvm.ac.in (P.N.); vamsi18@iisertvm.ac.in (S.V.K.I.)

* Correspondence: siva@iisertvm.ac.in

Abstract: We theoretically study the nonadiabatic relaxation dynamics of low-lying singlet excited-states of semisaturated planar tetracoordinated carbon molecule, C_7H_4 . This molecule possesses a stable C_{2v} ground-state equilibrium geometry. The three low-lying singlet states, S_1 , S_2 and S_3 , lie in the energy gap of about 1.2 eV. The potential energy surfaces constructed within the quadratic vibronic coupling formalism reveal multiple conical intersections in the Franck-Condon region. Upon photoexcitation to S_3 , the wavepacket decays rapidly to lower states via these conical intersections. We also observe the wavepacket transfer to S_3 during the initial wavepacket evolution on lower states, suggesting the nonadiabatic behavior of photoexcited planar C_7H_4 .

Keywords: excited-states; nonadiabatic dynamics; relaxation pathways



Citation: Jayakumari, C.M.; Nag, P.; Isukapalli, S.V.K.; Vennapusa, S.R. Exploring the Excited-State Nonadiabatic Effects in the Semisaturated Planar Tetracoordinated Carbon Molecule C_7H_4 . *Atoms* **2022**, *10*, 10. <https://doi.org/10.3390/atoms10010010>

Academic Editors: Venkatesan S. Thimmakondur and Krishnan Thirumoorthy

Received: 22 December 2021

Accepted: 15 January 2022

Published: 19 January 2022

Publisher's Note: MDPI stays neutral with regard to jurisdictional claims in published maps and institutional affiliations.



Copyright: © 2022 by the authors. Licensee MDPI, Basel, Switzerland. This article is an open access article distributed under the terms and conditions of the Creative Commons Attribution (CC BY) license (<https://creativecommons.org/licenses/by/4.0/>).

1. Introduction

The ongoing research in planar tetracoordinated carbon (ptC) for over five decades has opened a new era in the chemistry of carbon. Molecules containing ptC or even higher coordination have been successfully suggested and synthesized. The deviation from the long-established concept of tetrahedral tetracoordinate carbon by van't Hoff [1] and Le Bel [2] has raised the curiosity of researchers. Designing systems containing a planar tetracoordinated carbon center has remained a challenging task. The lone pair of electrons on the central ptC and the electron-deficient 3-centered 2-electron bonds make ptC unstable. The concept of ptC was first introduced by Monkhorst in 1968 [3]. Subsequently, using a planar methane model, Hoffmann and coworkers proposed strategies for stabilizing planar tetracoordinated carbon arrangements by electronic effects as well as steric effects [4,5].

Using those strategies, a number of molecules were proposed theoretically [6–16], though only a few were identified in the laboratory [17–21]. Merino and coworkers have reported a series of semisaturated ptC candidates containing cyclic hydrocarbons, which were created by combining C_5^{2-} moiety with saturated hydrocarbon fragments [22]. These were the first semisaturated cycles, containing a ptC stabilized only by electronic factors. The authors analyzed various ground-state properties, and they inferred that the multicentric nature of the bonding within the C_5^{2-} skeleton and the resulting electron delocalization provides stability to these molecules.

Although several studies have focussed on the various ground-state properties of ptCs, the excited-state properties of these molecules remain unexplored. In the present work, we focus on elucidating the excited-state dynamics of the semisaturated ptC, C_7H_4 (tricyclo[4.1.0.0^{1,3}]hept-2,6-diene-2,7-diyl) (cf., Figure 1), using combined electronic structure computations and quantum dynamics simulations. We generate the potential energy surfaces (PESs) of low-lying singlet excited electronic states within the quadratic vibronic coupling (QVC) framework. Subsequently, we perform quantum-mechanical wavepacket simulations within the well-established multidimensional configurational time-dependent Hartree (MCTDH) method. Finally, we analyze the electronic populations and reduced

nuclear densities and various stationary points of PESs to gain insights into the excited-state relaxation decay channels of the ptC molecule, C_7H_4 .

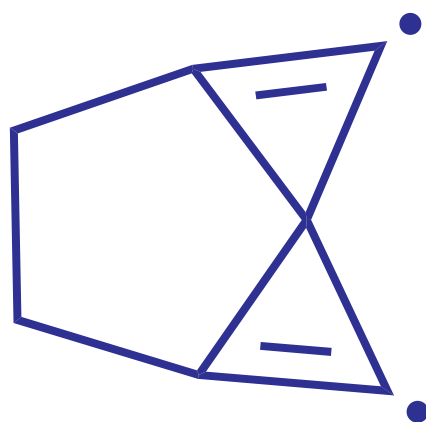


Figure 1. Structure of C_7H_4 .

2. Theoretical Framework

2.1. Electronic Structure Calculations

We perform the optimization and frequency computations associated with the ground-state equilibrium geometry of C_7H_4 within the density functional theory (DFT) using gas-phase conditions. These computations use the B3LYP [23]/6-311++G(d,p) level of theory. For excited-state computations, we rely on the time-dependent variant of DFT (TDDFT). We obtain vertical excitation energies and corresponding oscillator strengths using the long-range corrected ω B97XD functional (0.22 HF at short-range and 1.00 HF at long-range) [24] in combination with 6-311++G(d,p) basis set. All the calculations are done using Gaussian 16 program package [25].

To verify the suitability of the selected functional, we have done benchmarking calculations of excited-states with various quantum chemical methods. Accordingly, we employ time-dependent variants of B3LYP (containing 0.20 Hartree–Fock (HF) exchange), CAM-B3LYP [26] (comprises of 0.19 HF exchange at short-range, and 0.65 HF at long-range), LC- ω PBE [27] (no HF exchange at short-range and 1.00 HF at long-range) and M06-2X (comprises of 0.54 HF exchange) [28]. We use the 6-311++G(d,p) basis set for these computations. Further, we also evaluate excited-state energies using post-HF methods: equation of motion coupled cluster with single and double excitations (EOM-CCSD) method [29,30], resolution-of-the-identity second-order approximate coupled-cluster singles and doubles (RI-CC2) method [31], and algebraic diagrammatic construction method to second-order (ADC(2)) method [32]. These computations use the correlation consistent polarized valence double zeta (cc-pVDZ) basis set. The geometry optimized at the B3LYP/6-311++G(d,p) level of theory was used for all the above computations. We employ Gaussian 16 software package for TDDFT and EOM-CCSD computations and TURBOMOLE 7.4 software [33] for ADC(2) and RI-CC2 computations.

2.2. Vibronic Hamiltonian

Based on the computed vertical excitation energies, we are interested in studying the excited-state dynamics of the first three singlet excited-states of C_7H_4 . For this, we construct a 3×3 vibronic Hamiltonian based on the well-established QVC approach [34]. The Hamiltonian can be expressed as:

$$\mathcal{H} = (T_N + V_0)\mathbf{1}_3 + \begin{pmatrix} E_{S_1}^0 + \sum_{i \in a_1} \kappa_i^{(S_1)} Q_i + \frac{1}{2} \sum_{i \in a_1} \gamma_i^{(S_1)} Q_i^2 & \sum_{i \in a_1} \lambda_i^{(S_1-S_2)} Q_i & \sum_{j \in a_2} \lambda_j^{(S_1-S_3)} Q_j \\ h.c. & E_{S_2}^0 + \sum_{i \in a_1} \kappa_i^{(S_2)} Q_i + \frac{1}{2} \sum_{i \in a_1} \gamma_i^{(S_2)} Q_i^2 & \sum_{j \in a_2} \lambda_j^{(S_2-S_3)} Q_j \\ & & E_{S_3}^0 + \sum_{i \in a_1} \kappa_i^{(S_3)} Q_i + \frac{1}{2} \sum_{i \in a_1} \gamma_i^{(S_3)} Q_i^2 \end{pmatrix} \quad (1)$$

Here, T_N and V_0 are the ground-state kinetic energy and potential energy operators and are expressed in terms of the dimensionless normal coordinate (Q) within the harmonic approximation. E_m^0 represents the vertical excitation energy of the excited-states (for S_m , $m = 1, 2$ and 3). κ_i and γ_i denotes the linear and quadratic intrastate coupling parameters, respectively, along the totally symmetric vibrational mode, i . λ_j is the interstate coupling parameter along the non-totally symmetric vibrational mode, j . The interstate coupling constants between states of same symmetry (S_1 and S_2) are computed along the totally symmetric vibrational mode, a_1 , and is represented as λ_i . These coupling parameters are evaluated using the following expressions:

$$\kappa^{(S_m)} = \frac{\partial V_{S_m}}{\partial Q_i} \Big|_{Q_0}, \quad i \in a_1 \quad (2)$$

$$\gamma^{(S_m)} = \frac{\partial^2 V_{S_m}}{\partial Q_i^2} \Big|_{Q_0}, \quad i \in a_1 \quad (3)$$

$$\lambda_{i/j}^{(S_m-S_n)} = \left[\frac{1}{8} \frac{\partial^2}{\partial Q_{i/j}^2} |V_{S_m}(Q) - V_{S_n}(Q)|^2 \right]_{Q_0}^{1/2}, \quad i \in a_1; j \in a_2 \quad (4)$$

where, V_{S_m} and V_{S_n} are the adiabatic potential energies of two different electronic states, S_n and S_m , respectively; Q_0 represents the ground-state equilibrium geometry of the molecule.

2.3. Dynamics Simulations

We simulate the quantum nuclear dynamics of the singlet excited-states of C_7H_4 by using multiconfiguration time-dependent Hartree (MCTDH) approach [35–37] which is designed to solve the time-dependent Schrodinger equation for multidimensional dynamical systems. In this method, the nuclear wavefunction, Ψ , of a system with f degrees of freedom (DOF) is expressed as:

$$\Psi(Q_1, \dots, Q_f, t) = \sum_{i_1=1}^{n_1}, \dots, \sum_{i_f=1}^{n_f} R_{i_1, \dots, i_f}(t) \prod_{k=1}^f \phi_{i_k}^{(k)}(Q_k, t). \quad (5)$$

where Q_1, \dots, Q_f are the nuclear coordinates of vibrational modes. R_{i_1, \dots, i_f} and $\phi_{i_k}^{(k)}$ denote the MCTDH expansion coefficients and single-particle functions (SPFs), respectively. n_k represents the number of SPFs to describe the k -th DOF.

To reduce the memory requirement of the above treatment, we adopt a “mode combination” technique in which SPFs that can describe a set of DOF are used. The nuclear wavefunction can be then rewritten as a multi-configuration over p generalized particles:

$$\Psi(Q'_1, Q'_2, \dots, Q'_f, t) = \sum_{j_1=1}^{n_1}, \dots, \sum_{j_p=1}^{n_p} R_{j_1, \dots, j_p}(t) \phi_{j_1}^{(1)}(Q'_1, t), \dots, \phi_{j_p}^{(p)}(Q'_p, t) \quad (6)$$

with

$$\phi_j^{(k)}(Q'_k, t) = \phi_j^{(k)}(Q_1, Q_2, \dots, Q_w, t) \quad (7)$$

where $Q'_k = (Q_1, Q_2, \dots, Q_w)$ represents the multidimensional coordinate for mode k .

Out of the 28 degrees of freedom (27 vibrational modes and a set of electronic states) of C_7H_4 , a total of 14 (9 a_1 and 5 a_2) modes were selected based on the excitation strength of the modes. It is to be noted that S_1 – S_3 and S_2 – S_3 couplings are along a_2 modes and coupling between S_1 and S_2 , belonging to the same symmetry, are along a_1 modes. The nuclear wavepacket generated on S_3 PES has been propagated for 300 fs with a time step of 1 fs. The diabatic electronic populations and nuclear densities are then extracted to study the internal conversion dynamics. The Heidelberg MCTDH code version 8.5 Revision 11 [38] is employed for these calculations. Details of MCTDH dynamics such as mode combination, primitive basis, and SPFs are given in Supplementary Materials.

3. Results and Discussion

3.1. PESs and Conical Intersections

We collect the vertical excitation energies, oscillator strengths and symmetries of low-lying singlet excited-states of C_7H_4 computed at different levels of theory in Table 1. All computational methods yield the same electronic symmetries for S_1 and S_2 . We also note that all methods predict B_2 symmetry for S_3 except TD-B3LYP and TD-M06-2X. The latter two methods show A_1 symmetry for this state. Concerning oscillator strengths, all methods predict a smaller value for S_1 than higher electronic states. Here, the important feature of Table 1 is the S_1 – S_3 energy gap; all methods predict a gap of about 1.2 eV. As these states lie within this energy gap, one would expect the molecule to follow nonadiabatic behavior upon photoexcitation. As the vertical energies (as well as the oscillator strengths) of the excited-states computed at the ω B97XD/6-311++G(d,p) level of theory match well with the computationally expensive wavefunction methods, we perform all calculations using this method.

Table 1. Vertical excitation energies of C_7H_4 computed using different levels of theory. 6-311++G(d,p) is the basis set used for the TDDFT methods and cc-pVDZ is used for the wavefunction based methods.

Methods	S_1	S_2	S_3
TD- ω B97XD	4.3417 (B_1 , 0.001)	4.8192 (B_1 , 0.043)	5.5606 (B_2 , 0.049)
TD-B3LYP	4.0221 (B_1 , 0.005)	4.5325 (B_1 , 0.032)	5.0136 (A_1 , 0.010)
TD-CAMB3LYP	4.3389 (B_1 , 0.001)	4.7960 (B_1 , 0.045)	5.5310 (B_2 , 0.045)
TD-LC- ω PBE	4.5102 (B_1 , 0.000)	4.9985 (B_1 , 0.050)	5.7237 (B_2 , 0.037)
TD-M06-2X	4.2035 (B_1 , 0.000)	4.5731 (B_1 , 0.039)	5.4983 (A_1 , 0.004)
EOM-CCSD	4.3121 (B_1 , 0.002)	4.9658 (B_1 , 0.032)	5.5197 (B_2 , 0.031)
ADC(2)	4.3239 (B_1 , 0.003)	4.9202 (B_1 , 0.030)	5.4091 (B_2 , 0.042)
RICC2	4.2634 (B_1 , 0.004)	4.8697 (B_1 , 0.027)	5.3844 (B_2 , 0.046)

To explore the nuclear dependence of these electronic states, we plot adiabatic potential energy profiles (solid lines) against in-plane ring deformation vibrational coordinates (Q_{15}) in Figure 2. The ab initio energies (plus harmonic potential) are shown as filled circles in this figure. We observe that the potential energy profiles generated within the QVC approach reproduce the ab initio energies quite well, confirming the suitability of the latter approach to study the dynamics happening within the Franck-Condon (FC) region. We observe multiple curve crossings between the excited- states of interest. Such crossings also occur in the other vibrational coordinate space, however those data are not shown here for brevity. It should be mentioned that these crossings would form the seam of conical intersection in the multidimensional space. Figure 3 depicts the conical intersections associated with the adiabatic PESs of S_1 , S_2 , and S_3 states along the coordinates of ring deformation (Q_{15}) and C=C stretch (Q_{22}) vibrations. These vibrational modes are represented in Figure 4.

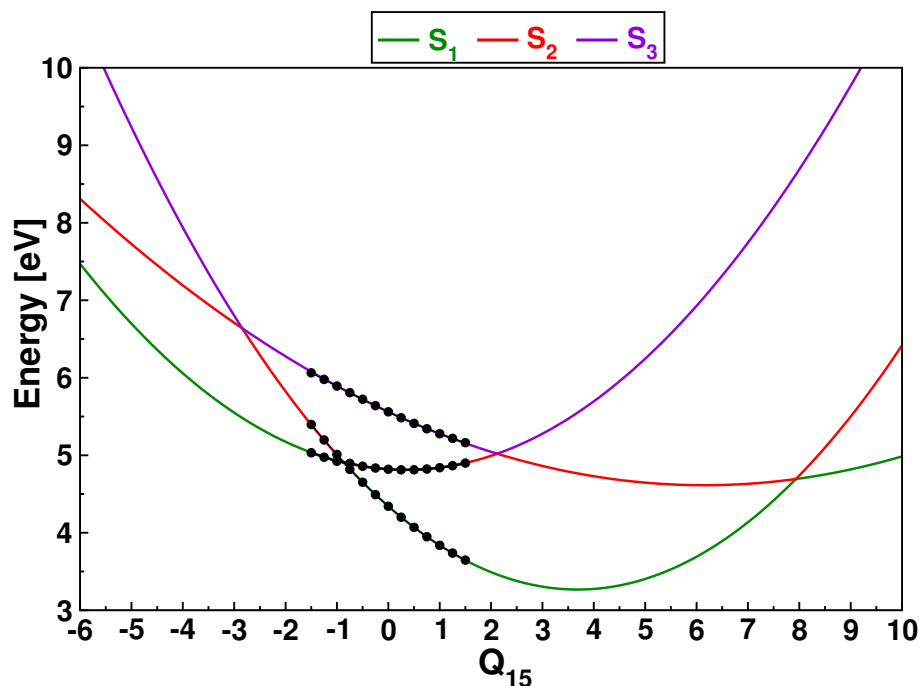


Figure 2. Computed adiabatic potential energy curves of along Q_{15} of C_7H_4 within the QVC approach. The solid circles represent the ab initio points plus ground-state harmonic potential energy.

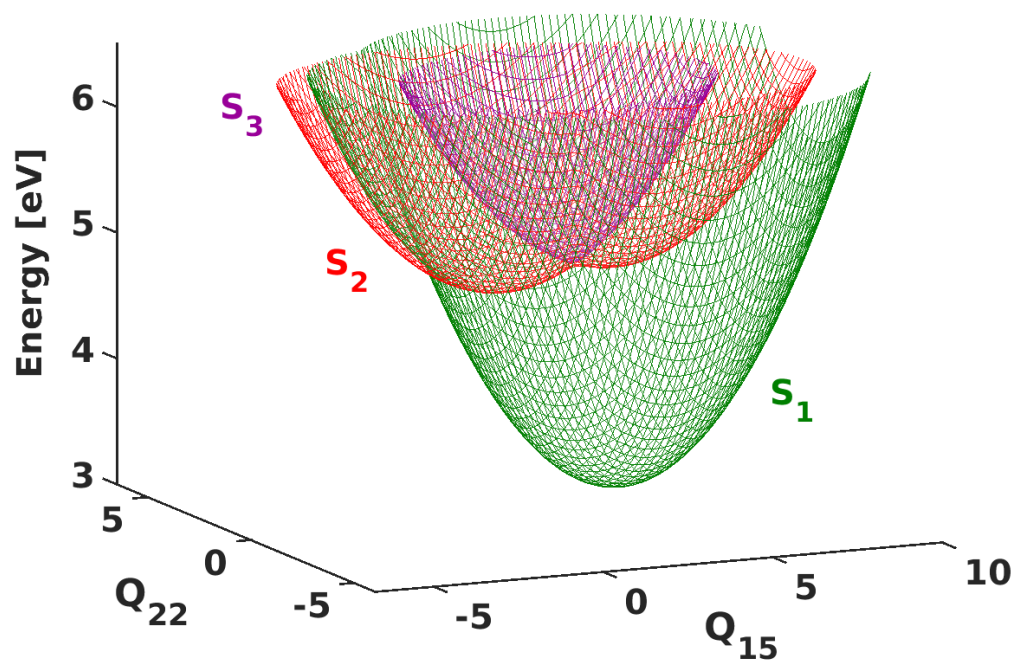


Figure 3. Adiabatic potential energy surfaces of C_7H_4 in the Q_{15} and Q_{22} vibrational space computed within the QVC approach.

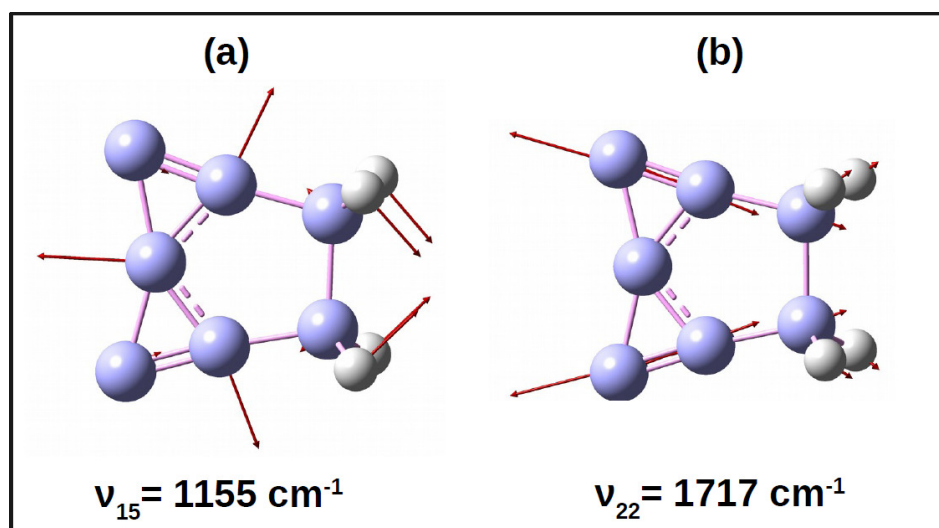


Figure 4. Schematic representation of the (a) in-plane ring deformation (Q_{15}) and (b) C=C stretch (Q_{22}) vibrational modes of C_7H_4 . Harmonic frequencies obtained using B3LYP/6-311++G(d,p) level of theory are also shown.

We also evaluate two other important quantities: minimum energy conical intersection and equilibrium minimum of excited-states. These quantities are crucial to explain the wavepacket dynamics happening on the coupled S_1 – S_2 – S_3 PESs. Following expressions are employed to evaluate those quantities: [39]

$$MECI = a + \frac{(b - c)^2}{2d} - \frac{1}{2} \sum_{i=1}^N \frac{\sigma_i^2}{\omega_i} \quad (8)$$

where,

$$a = \frac{E_1^0 + E_2^0}{2} \quad (9)$$

$$c = \frac{E_2^0 - E_1^0}{2} \quad (10)$$

$$b = \sum_{i=1}^N \frac{\delta_i \sigma_i}{\omega_i} \quad (11)$$

$$d = \sum_{i=1}^N \frac{\delta_i^2}{\omega_i} \quad (12)$$

$$\sigma_i = \frac{\kappa_i^{(2)} + \kappa_i^{(1)}}{2} \quad (13)$$

$$\delta_i = \frac{\kappa_i^{(2)} - \kappa_i^{(1)}}{2} \quad (14)$$

$$E_m^{\min} = E_m^0 - \frac{1}{2} \sum_{i=1}^N \frac{\kappa_i^2}{\omega_i} \quad (15)$$

where ω_i is the harmonic frequency of the i th totally symmetric vibrational mode and N is the total number of such modes.

The molecule might display unexpected nonradiative decay dynamics due to the presence of accessible conical intersections within the FC region (cf., Table 2). For instance, the S_2 – S_3 conical intersection lies ~ 0.5 eV below the FC point of S_3 (cf., Tables 1 and 2). Hence, upon excitation to S_3 , the molecule can, in principle, decay rapidly via this conical intersection. We expect this intersection point and the S_1 – S_3 conical intersection,

that lies slightly above (~ 0.1 eV) the FC point of S_3 , might play an important role in the decay dynamics.

Table 2. Relevant stationary points (state minima and MECI) on the coupled S_1 – S_2 – S_3 PESs of C_7H_4 .

Stationary Point	Energy (eV)
S_1^{\min}	3.6039
S_2^{\min}	4.7940
S_3^{\min}	4.3006
S_1/S_2	4.7970
S_1/S_3	5.6376
S_2/S_3	5.0552

3.2. Singlet Dynamics

To investigate the fate of C_7H_4 in the higher excited singlet states, we perform dynamics simulations by launching the initial wavepacket at the FC point of the “bright” S_3 . Figure 5a collects the time-dependent electronic population profiles obtained from this wavepacket propagation calculation. We observe a rapid population transfer from S_3 to S_2 . The wavepacket evolving on S_3 could easily access the S_2/S_3 MECI (~ 5.06 eV, cf., Table 2) and thus promote rapid nonadiabatic population transfer.

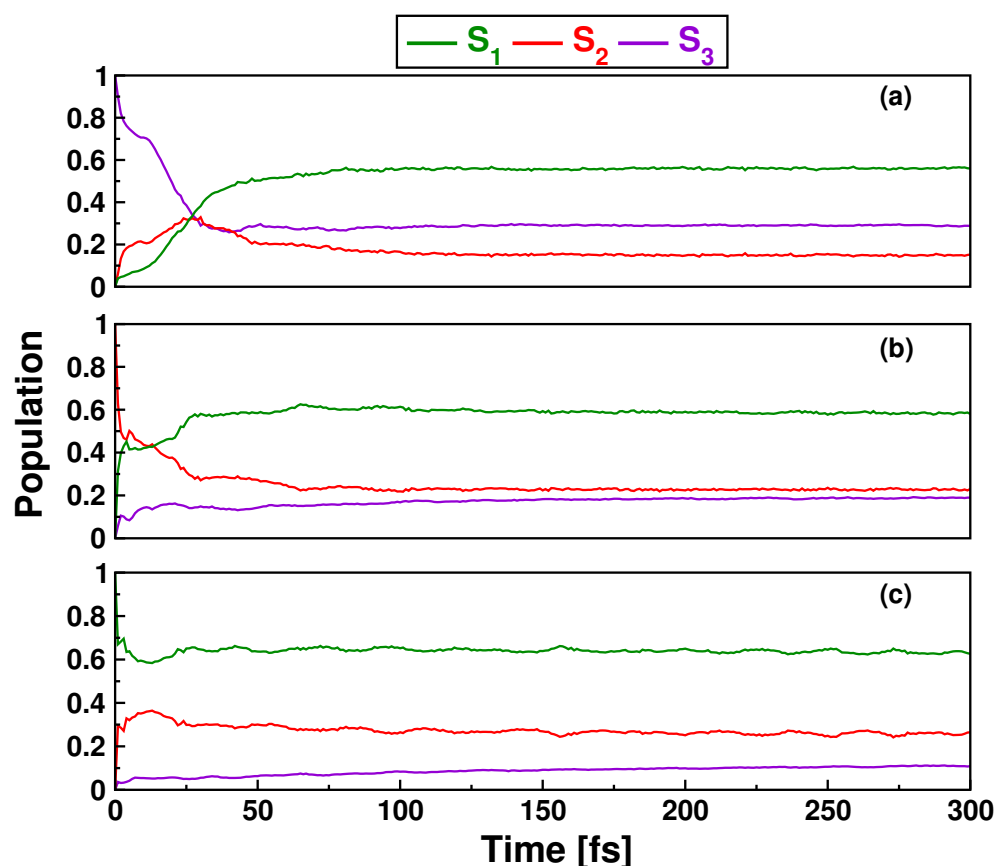


Figure 5. Diabatic electronic population profiles of singlet excited-states generated by propagation of initial wavepacket on (a) S_3 , (b) S_2 , and (c) S_1 of C_7H_4 .

We note that $\sim 70\%$ depopulation of S_3 happens within the first 40 fs of propagation time. We observe a sharp rise in the S_1 population during this period. This sharp rise would emerge from the wavepacket decay via S_1 – S_3 and S_1 – S_2 conical intersections. Interestingly, the populations of the involved states remain almost unchanged after 50 fs. These

observations suggest the remnant wavepacket localization at the respective equilibrium minimum of involved electronic states after the early nonadiabatic wavepacket transfer.

To further validate the nonadiabatic population transfer, we plot the reduced nuclear densities associated with the ring deformation mode, i.e., Q_{15} , for three electronic states in Figure 6. The density would be maximum on S_3 at $t=0$ fs as the wavepacket propagation starts on this state. We observe the rapid density reduction within 20 fs, and after that, the density remains unchanged until the end of propagation time. For S_2 , the density accumulates rapidly after a few femtoseconds and reaches a maximum at about 20 fs. After that, the density reduces up to 50 fs and remains unchanged till 300 fs. For S_1 , we observe a gradual increase of nuclear density, reaching a maximum value at about 20 fs. After that, the nuclear density on S_1 would remain unchanged up to 300 fs. From these observations, we infer that the wavepacket decay to S_1 would occur within a few tens of femtoseconds after photoexcitation to S_3 .

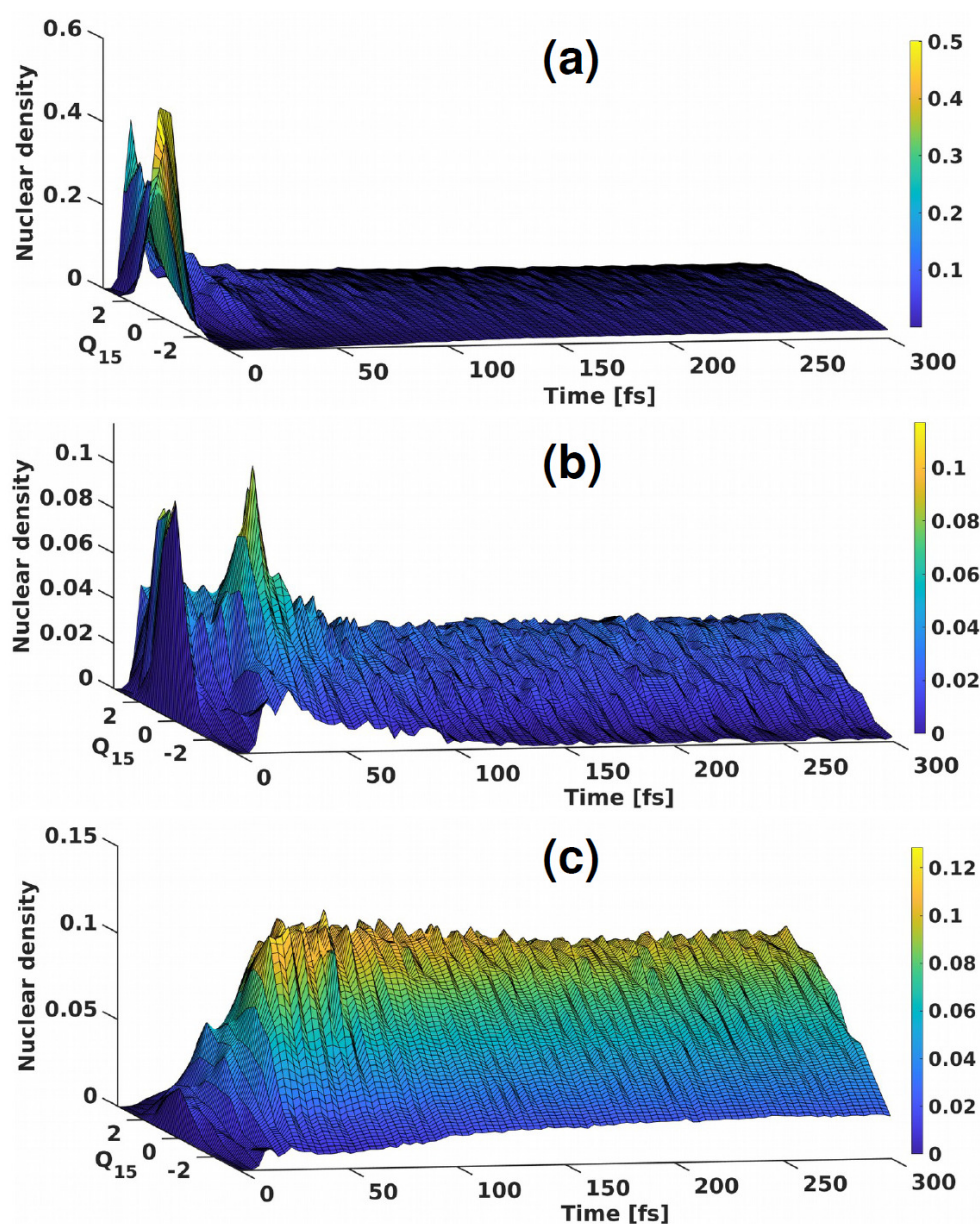


Figure 6. Nuclear densities variation of (a) S_3 , (b) S_2 , and (c) S_1 along Q_{15} of C_7H_4 , obtained by propagating initial wavepacket on the “bright” S_3 state.

Next, we launch the initial wavepacket at the FC point of S_2 and S_1 to explore the decay dynamics of individual electronic states. The accessible S_1/S_2 MECI (~ 4.80 eV, cf., Table 2) combined with the high interstate coupling via a_1 modes results in an extremely rapid population transfer from S_2 to S_1 (cf., Figure 5b). The S_1 population reaches an asymptotic value of ~ 0.6 at the end of 300 fs. A minor population transfer to S_3 can also be seen, attributed to the strong nonadiabatic coupling between S_2 and S_3 states.

The wavepacket propagated on the S_1 PES shows an appreciable decay ($\sim 40\%$) to S_2 till the initial 20 fs and further, remains constant (cf., Figure 5c). Such population profile suggests that the molecule might be trapped at the equilibrium minimum of S_1 , which is ~ 0.7 eV lower in energy from the S_1 FC point. The molecule could no longer access any conical intersections, resulting in no noticeable population transfer. Similar profile is also observed in the variation of nuclear densities (along Q_{15} vibrational mode) across the excited-states with the wavepacket evolving on S_1 (cf., Figure S1 in Supplementary Materials). It is noted that no state shows 100% decay within 300 fs. So dynamics simulations need to be conducted for a longer duration for the complete decay of the excited-states.

We note that the QVC model employed in this study would be helpful to gain insights into the FC dynamics. However, concerning the fluxional behavior of molecules containing ptC, it is necessary to adopt a theoretical model that involves possible excited-state dissociation pathways. Identifying such dissociative pathways through experimental investigations can be complicated due to nonadiabatic events occurring in the FC region. However, one could rely on the high-level on-the-fly dynamics simulations to study the photoproducts of ptC molecules.

4. Conclusions

In the present work, we provide vital insights on the nonadiabatic relaxation dynamics of the semisaturated ptC molecule, C_7H_4 . PESs constructed by employing QVC formalism revealed multiple conical intersections among the three singlet excited-states, S_1 , S_2 , and S_3 . The molecule excited to the optically “bright” S_3 returns to S_1 on an ultrafast timescale via these conical intersections. Similarly, these crossing points also promote the wavepacket transfer to higher states (S_2 and S_3) while the wavepacket is initially on S_1 , demonstrating the nonadiabatic behavior of C_7H_4 irrespective of excitation energy. Although the present study has provided essential features of excited-state decay dynamics, a detailed quantum dynamics study using the multi-reference configuration interaction (MRCI) or multiconfigurational quasidegenerate perturbation theory (MCQDPT) PESs is planned to provide an accurate picture of the relaxation pathways of C_7H_4 .

Supplementary Materials: The following supporting information can be downloaded at: <https://www.mdpi.com/article/10.3390/atoms10010010/s1>. Figure S1: Nuclear densities variation of the singlet excited states of C_7H_4 with the wavepacket evolving on S_1 state, Table S1: Harmonic vibrational frequencies of C_7H_4 calculated at B3LYP/6-311++G(d,p) level of theory, Table S2: Ground-state (S_0) equilibrium geometry of C_7H_4 optimized at B3LYP/6-311++G(d,p) level of theory, Table S3: Linear intrastate coupling parameters (κ) for the singlet electronic states of C_7H_4 calculated at (TD) ω B97XD/6-311++G(d,p) level of theory, Table S4: Quadratic intrastate coupling parameters (γ) for the singlet electronic states of C_7H_4 calculated at (TD) ω B97XD/6-311++G(d,p) level of theory, Table S5: Linear interstate coupling parameters (γ) computed along a_2 modes for the singlet electronic states of C_7H_4 calculated at (TD) ω B97XD/6-311++G(d,p) level of theory, Table S6: Linear interstate coupling parameters (γ) computed along a_1 modes for the singlet electronic states of C_7H_4 calculated at (TD) ω B97XD/6-311++G(d,p) level of theory, Table S7: MCTDH details of S_1 - S_2 - S_3 vibronic dynamics of C_7H_4 .

Author Contributions: Conceptualization, S.R.V.; methodology, S.R.V.; validation, S.R.V.; formal analysis, C.M.J., P.N. and S.V.K.I.; investigation, C.M.J., P.N. and S.V.K.I.; data curation, C.M.J., P.N. and S.V.K.I.; writing—original draft preparation, C.M.J.; writing—review and editing, S.R.V.; supervision, S.R.V. All authors have read and agreed to the published version of the manuscript.

Funding: This research received no external funding.

Data Availability Statement: Data is contained within the article or supplementary material.

Acknowledgments: C.M.J. acknowledges Council of Scientific and Industrial Research (CSIR), Government of India, for doctoral fellowship. P.N. thanks Ministry of Higher Education, Government of India, for the fellowship under the Prime Minister's Research Fellows (PMRF) scheme. S.V.K.I. (DST/INSPIRE/IF170980) thanks Department of Science and Technology, New Delhi, for DST-INSPIRE fellowship. All authors gratefully acknowledge IISER TVM for computational resources.

Conflicts of Interest: The authors declare no conflict of interest.

Abbreviations

The following abbreviations are used in this manuscript:

ptC	Planar tetracoordinated carbon
PES	Potential energy surface
QVC	Quadratic vibronic coupling
MCTDH	Multiconfiguration time-dependent hartree
TDDFT	Time-dependent density functional theory
EOM-CCSD	Equation of motion coupled cluster with single and double excitations
RI-CC2	Resolution-of-the-identity second-order approximate coupled-cluster singles and doubles
ADC(2)	Algebraic diagrammatic construction method to second-order
FC	Franck-Condon
MECI	Minimum energy conical intersection

References

1. van't Hoff, J.H. A suggestion looking to the extension into space of the structural formulas at present used in chemistry, and a note upon the relation between the optical activity and the chemical constitution of organic compounds. *Arch. Neerl. Sci. Exact Nat.* **1874**, *9*, 445–454.
2. Le Bel, J. On the relations which exist between the atomic formulas of organic compounds and the rotatory power of their solutions. *Bull. Soc. Chim.* **1874**, *22*, 337–347.
3. Monkhurst, H.J. Activation energy for interconversion of enantiomers containing an asymmetric carbon atom without breaking bonds. *Chem. Commun.* **1968**, *11*, 1111–1112. [[CrossRef](#)]
4. Hoffmann, R.; Alder, R.W.; Wilcox, C.F. Planar tetracoordinate carbon. *J. Am. Chem. Soc.* **1970**, *92*, 4992–4993. [[CrossRef](#)]
5. Hoffmann, R. The theoretical design of novel stabilized systems. *Pure Appl. Chem.* **1971**, *28*, 181–194. [[CrossRef](#)]
6. McGrath, M.P.; Radom, L. Alkaplanes: a class of neutral hydrocarbons containing a potentially planar tetracoordinate carbon. *J. Am. Chem. Soc.* **1993**, *115*, 3320–3321. [[CrossRef](#)]
7. Lyons, J.E.; Rasmussen, D.R.; McGrath, M.P.; Nobes, R.H.; Radom, L. Octaplane: A saturated hydrocarbon with a remarkably low ionization energy leading to a cation with a planar tetracoordinate carbon atom. *Angew. Chem. Int. Ed. Engl.* **1994**, *33*, 1667–1668. [[CrossRef](#)]
8. Sorger, K.; Schleyer, P.v.R. Planar and inherently non-tetrahedral tetracoordinate carbon: A status report. *J. Mol. Struct. Theochem* **1995**, *338*, 317–346. [[CrossRef](#)]
9. Röttger, D.; Erker, G. Compounds Containing Planar-Tetracoordinate Carbon. *Angew. Chem. Int. Ed. Engl.* **1997**, *36*, 812–827. [[CrossRef](#)]
10. Radom, L.; Rasmussen, D.R. The planar carbon story. *Pure Appl. Chem.* **1998**, *70*, 1977–1984. [[CrossRef](#)]
11. Siebert, W.; Gunale, A. Compounds containing a planar-tetracoordinate carbon atom as analogues of planar methane. *Chem. Soc. Rev.* **1999**, *28*, 367–371. [[CrossRef](#)]
12. Rasmussen, D.R.; Radom, L. Planar-Tetracoordinate Carbon in a Neutral Saturated Hydrocarbon: Theoretical Design and Characterization. *Angew. Chem. Int. Ed.* **1999**, *38*, 2875–2878. [[CrossRef](#)]
13. Rasmussen, D.R.; Radom, L. Hemispiroalkaplanes: Hydrocarbon Cage Systems with a Pyramidal-Tetracoordinate Carbon Atom and Remarkable Basicity. *Chem. A Eur. J.* **2000**, *6*, 2470–2483. [[CrossRef](#)]
14. Priyakumar, U.D.; Sastry, G.N. A system with three contiguous planar tetracoordinate carbons is viable: a computational study on a C₆H₆= isomer. *Tetrahedron Lett.* **2004**, *45*, 1515–1517. [[CrossRef](#)]
15. Perez, N.; Heine, T.; Barthel, R.; Seifert, G.; Vela, A.; Mendez-Rojas, M.A.; Merino, G. Planar tetracoordinate carbons in cyclic hydrocarbons. *Org. Lett.* **2005**, *7*, 1509–1512. [[CrossRef](#)]
16. Merino, G.; Méndez-Rojas, M.A.; Vela, A.; Heine, T. Recent advances in planar tetracoordinate carbon chemistry. *J. Comput. Chem.* **2007**, *28*, 362–372. [[CrossRef](#)]
17. Li, X.; Wang, L.S.; Boldyrev, A.I.; Simons, J. Tetracoordinated planar carbon in the Al₄C-anion. A combined photoelectron spectroscopy and ab initio study. *J. Am. Chem. Soc.* **1999**, *121*, 6033–6038. [[CrossRef](#)]

18. Li, X.; Zhang, H.; Wang, L.; Geske, G.; Boldyrev, A. ZUSCHRIFTEN-Pentaatomic Tetracoordinate Planar Carbon,(CA14) 2-: A New Structural Unit and Its Salt Complexes Stichwörter: Ab-initio-Rechnungen. Aluminium. Charge-Transfer Koordinationschemie. *Angew.-Chem.-Ger. Ed.* **2000**, *112*, 3776–3778. [CrossRef]
19. Wang, L.S.; Boldyrev, A.I.; Li, X.; Simons, J. Experimental observation of pentaatomic tetracoordinate planar carbon-containing molecules. *J. Am. Chem. Soc.* **2000**, *122*, 7681–7687. [CrossRef]
20. Li, X.; Zhai, H.J.; Wang, L.S. Photoelectron spectroscopy of pentaatomic tetracoordinate planar carbon molecules: CA13Si- and CA13Ge-. *Chem. Phys. Lett.* **2002**, *357*, 415–419. [CrossRef]
21. Xu, J.; Zhang, X.; Yu, S.; Ding, Y.h.; Bowen, K.H. Identifying the Hydrogenated Planar Tetracoordinate Carbon: A Combined Experimental and Theoretical Study of CA14H and CA14H-. *J. Phys. Chem. Lett.* **2017**, *8*, 2263–2267. [CrossRef] [PubMed]
22. Perez-Peralta, N.; Sanchez, M.; Martin-Polo, J.; Islas, R.; Vela, A.; Merino, G. Planar Tetracoordinate Carbons in Cyclic Semisaturated Hydrocarbons. *J. Org. Chem.* **2008**, *73*, 7037–7044. [CrossRef] [PubMed]
23. Becke, A.D. Density-functional thermochemistry. III. The role of exact exchange. *J. Chem. Phys.* **1993**, *98*, 5648–5652. [CrossRef]
24. Chai, J.D.; Head-Gordon, M. Long-range corrected hybrid density functionals with damped atom–atom dispersion corrections. *Phys. Chem. Chem. Phys.* **2008**, *10*, 6615–6620. [CrossRef]
25. Frisch, M.J.; Trucks, G.W.; Schlegel, H.B.; Scuseria, G.E.; Robb, M.A.; Cheeseman, J.R.; Scalmani, G.; Barone, V.; Petersson, G.A.; Nakatsuji, H.; et al. *Gaussian 16 Revision C.01*; Gaussian Inc.: Wallingford, CT, USA, 2016.
26. Yanai, T.; Tew, D.P.; Handy, N.C. A new hybrid exchange–correlation functional using the Coulomb-attenuating method (CAM-B3LYP). *Chem. Phys. Lett.* **2004**, *393*, 51–57. [CrossRef]
27. Tawada, Y.; Tsuneda, T.; Yanagisawa, S.; Yanai, T.; Hirao, K. A long-range-corrected time-dependent density functional theory. *J. Chem. Phys.* **2004**, *120*, 8425–8433. [CrossRef] [PubMed]
28. Zhao, Y.; Truhlar, D.G. Comparative DFT Study of van der Waals Complexes: Rare-Gas Dimers, Alkaline-Earth Dimers, Zinc Dimer, and Zinc-Rare-Gas Dimers. *J. Phys. Chem. A* **2006**, *110*, 5121–5129. [CrossRef]
29. Sekino, H.; Bartlett, R.J. A linear response, coupled-cluster theory for excitation energy. *Int. J. Quantum Chem.* **1984**, *26*, 255–265. [CrossRef]
30. Stanton, J.F.; Bartlett, R.J. The equation of motion coupled-cluster method. A systematic biorthogonal approach to molecular excitation energies, transition probabilities, and excited state properties. *J. Chem. Phys.* **1993**, *98*, 7029–7039. [CrossRef]
31. Hättig, C.; Weigend, F. CC2 excitation energy calculations on large molecules using the resolution of the identity approximation. *J. Chem. Phys.* **2000**, *113*, 5154–5161. [CrossRef]
32. Trofimov, A.; Krivdina, I.; Weller, J.; Schirmer, J. Algebraic-diagrammatic construction propagator approach to molecular response properties. *Chem. Phys.* **2006**, *329*, 1–10. [CrossRef]
33. TURBOMOLE V7.4 2019, a Development of University of Karlsruhe and Forschungszentrum Karlsruhe GmbH, 1989–2007. TURBOMOLE GmbH, Since 2007. Available online: <http://www.turbomole.com> (accessed on 11 August 2021).
34. Domcke, W.; Yarkony, D.R.; Köppel, H. *Conical Intersections*; World Scientific: Singapore, 2004. [CrossRef]
35. Meyer, H.D.; Manthe, U.; Cederbaum, L. The multi-configurational time-dependent Hartree approach. *Chem. Phys. Lett.* **1990**, *165*, 73–78. [CrossRef]
36. Manthe, U.; Meyer, H.; Cederbaum, L.S. Wave-packet dynamics within the multiconfiguration Hartree framework: General aspects and application to NOCl. *J. Chem. Phys.* **1992**, *97*, 3199–3213. [CrossRef]
37. Beck, M.; Jäckle, A.; Worth, G.; Meyer, H.D. The multiconfiguration time-dependent Hartree (MCTDH) method: A highly efficient algorithm for propagating wavepackets. *Phys. Rep.* **2000**, *324*, 1–105. [CrossRef]
38. Worth, G.A.; Beck, M.H.; Jäckle, A.; Meyer, H.D. The MCTDH Package, Version 8.5. 2019. Available online: <http://mctdh.uni-hd.de> (accessed on 21 April 2021).
39. Köppel, H.; Domcke, W.; Cederbaum, L.S. Multimode Molecular Dynamics Beyond the Born-Oppenheimer Approximation. In *Advances in Chemical Physics*; John Wiley & Sons, Ltd.: Amsterdam, The Netherlands, 1984; pp. 59–246. [CrossRef]